Structural and Ion Dynamics in Fluorine-Free Oligoether Carboxylate Ionic Liquid-Based Electrolytes

THE JOURNAL OF PHYSICAL CHEMISTRY B

pubs.acs.org/JPCB

Article

Structural and Ion Dynamics in Fluorine-Free Oligoether Carboxylate Ionic Liquid-Based Electrolytes

Faiz Ullah Shah,* Oleg I. Gnezdilov, Inayat Ali Khan, Andrei Filippov, Natalia A. Slad, and Patrik Johansson*

Cite This: *J. Phys. Chem. B* 2020, 124, 9690–9700

Read Online

ACCESS | Metrics & More | Article Recommendations | Supporting Information

ABSTRACT: Here, we investigate the physicochemical and electrochemical properties of fluorine-free ionic liquid (IL)-based electrolytes with two different cations, tetrabutylphosphonium, $(P_{4,4,4,4})^+$, and tetrabutylammonium, $(N_{4,4,4,4})^+$, coupled to a new anion, 2-[2-(2-methoxyethoxy)ethoxy]acetate anion $(MEEA)^-$, for both neat and $(P_{4,4,4,4})(MEEA)$ also doped with 10−40 mol % of Li(MEEA). We find relatively weaker cation−anion interactions in $(P_{4,4,4,4})(MEEA)$ than in $(N_{4,4,4,4})(MEEA)$, and for both ILs, the structural flexibility of the oligoether functionality in the anion results in low glass transition temperatures, also for the electrolytes made. The pulsed field gradient nuclear magnetic resonance (PFG NMR) data suggest faster diffusion of the $(MEEA)^-$ anion than $(P_{4,4,4,4})^+$ cation in the neat IL, but the addition of a Li salt results in slightly lower mobility of the former than the latter and lower ionic conductivity. This agrees with the combined ^{7}Li NMR and attenuated total reflection−Fourier transform infrared (ATR−FTIR) spectroscopy data, which unambiguously reveal preferential interactions between the lithium cations and the carboxylate groups of the IL anions, which also increased as a function of the lithium salt concentration. In total, these systems provide a stepping stone for further design of fluorine-free and low glass transition temperature IL-based electrolytes and also stress how crucial it is to control the strength of ion−ion interactions.

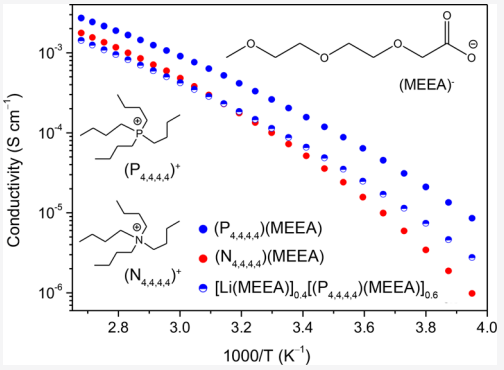

INTRODUCTION

The liquid electrolytes used in conventional lithium-ion batteries (LIBs) are most often composed of the salt lithium hexafluorophosphate ($LiPF_6$), or sometimes lithium tetrafluoroborate ($LiBF_4$), salts that dissolve in flammable carbonate-based organic solvents.[1,2] Such electrolytes have a number of drawbacks adversely affecting the battery performance when used and also cause difficulties at the recycling stage. The most problematic properties are they are intrinsically flammable, have unsatisfactory electrochemical stability windows (ESWs), not the least for future high-voltage LIBs, and have limited thermal stability. A particularly problematic aspect of the latter is the decomposition of $LiPF_6$ at elevated temperatures producing lithium fluoride (LiF) and phosphorous pentafluoride (PF_5), the latter forming toxic hydrofluoric acid (HF)—a serious hazard that must be dealt with.[3] Taken altogether, this urges for extensive research to develop thermally and electrochemically stable, but still performant, electrolytes to replace the conventional organic solvent-based electrolytes.

Among the organic solvent-based electrolytes studied, different oligoethers (also known as "glymes") have been extensively studied over the past decades, much due to their desirable physicochemical properties.[4] Oligoethers is a class of organic compounds with the general chemical formula, [R−$(OCH_2CH_2)_n$−OR], that often are abbreviated as G*n* where "*n*" represents the number of repeating units and denoted as monoglyme (G1), diglyme (G2), triglyme (G3), tetraglyme (G4), etc.[5] As compared to carbonate-based organic solvents, glymes have higher flash points and better solubility for lithium salts[6]—they can even dissolve an equimolar amount of lithium salt via an ether multidentate coordination functionality making complexes known as solvate ionic liquids (SILs) as they mimic ionic liquids (ILs) with high thermal and electrochemical stabilities and high ionic conductivities.[7,8] Such alkali ion−glyme complexes can even be reversibly intercalated inside graphite electrodes to enable charge storage based on solvent cointercalation.[9,10] Tetraglymes have been suggested to be stable against nucleophilic attack by superoxides and therefore are used in electrolytes for lithium−air batteries.[11] As they also form very thin and flexible solid electrolyte interphase (SEI) layers on highly reactive alkali metal anode surfaces, they are also considered for next-

Received: May 26, 2020
Revised: September 21, 2020
Published: October 20, 2020

generation batteries (NGBs) such as lithium−air and lithium−sulfur batteries,[12] but they suffer from instability at high redox potentials.[13]

Here, we combine the features of glyme solvents with those of ILs. ILs have for long been used as promising electrolyte solvents for LIBs[14−16] and NGBs.[17,18] ILs are salts made entirely of cations and anions with a melting point below 100 °C, and most are liquid at room temperature: room temperature ionic liquids (RTILs). As touched upon briefly above, ILs/RTILs possess a combination of properties making them excellent bases for electrolytes such as a nonflammability, negligible vapor pressures, high chemical and thermal stabilities, inherent high ionic conductivities, and wide electrochemical stability windows (ESWs)—sometimes quoted up to 6.0 V.[19−21]

IL-based LIB electrolytes can thus arguably overcome some of the drawbacks of conventional liquid electrolytes. The most commonly studied IL-based LIB electrolytes use heavily fluorinated anions, bis(trifluoromethanesulfonyl)imide (TFSI) and more recently bis(fluorosulfonyl)imide (FSI).[22] Typically, these electrolytes are made by dissolving LiTFSI/LiFSI in ILs such as pyrrolidinium TFSI or imidazolium TFSI,[23] pyrrolidinium FSI,[24] morpholinium FSI,[25] piperidinium TFSI,[26] or phosphonium FSI.[27] The use of fluorinated anions, however, makes these electrolytes less stable and sensitive to moisture,[28] and thus fluorine-free IL-based electrolytes are highly desired.

We exploit a combination of oligoethers and ILs by creating ILs with tetraalkyl phosphonium, $(PR_4)^+$, and ammonium, $(NR_4)^+$, cations coupled to a new common fluorine-free oligoether-based anion, 2-[2-(2-methoxyethoxy)ethoxy]-acetate, $(MEEA)^-$, and the corresponding Li-salt, Li(MEEA) (Figure 1). The $(MEEA)^-$ anion is designed aiming at IL-based electrolytes with low glass transition temperatures, due to the presence of ethylene oxide units, which might enhance the flexibility of the alkyl chain, as previously demonstrated for IL cations.[29] The reason for using both $(N_{4,4,4,4})^+$ and $(P_{4,4,4,4})^+$ IL cations is that although the cationic central atoms are largely shielded by the alkyl chains, they still have a significant effect on the IL properties mainly due to the differences in charge density of the nitrogen (higher) and phosphorous (lower) atoms.[30] This was analyzed by Coutinho and co-workers using density functional theory (DFT) calculations for $(N_{4,4,4,6})(NTf_2)$ and $(P_{4,4,4,6})(NTf_2)$ ILs, and they found stronger Coulomb interactions and more positively charged connecting methylene groups, that is, a larger charge delocalization for the former cation.[31] This might have profound effects on everything from thermal, phase, and electrochemical stabilities as well as the local interactions and dynamics.

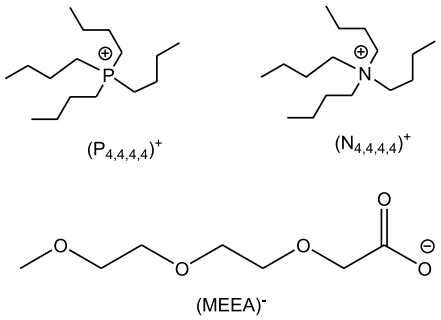

Figure 1. Chemical structures and acronyms for the ILs cations and anions.

A wide range of characterization techniques are employed here to study the physicochemical and electrochemical properties to enable a better understanding of the fundamental potential of these systems as LIB electrolytes.

EXPERIMENTAL SECTION

Electrolyte Preparation. The fluorine-free oligoether carboxylate-based Li-salt and ILs were synthesized by a slight modification of the procedure described earlier.[32] The synthesis protocols and material characterizations including multinuclear (^{1}H, ^{13}C, ^{7}Li, and ^{31}P) nuclear magnetic resonance (NMR) spectroscopy, mass spectrometry, and elemental analysis are described in detail in the Supporting Information. The electrolytes were prepared by mixing 10−50 mol % of Li(MEEA) in $(P_{4,4,4,4})$(MEEA) (Table 1), but phase separation was observed for the highest salt concentration and this is therefore not further included in this study. All the samples were kept in a vacuum oven at 80 °C for 3−6 days until the water content was less than 200 ppm as determined by the Karl Fischer titration using a 917 coulometer (Metrohm).

Table 1. Compositions and Abbreviations of the Electrolytes Made

electrolyte acronym	Li(MEEA) (mol %)	$(P_{4,4,4,4})$(MEEA) (mol %)	molality (mol kg^{-1})
$[Li(MEEA)]_{0.1}[(P_{4,4,4,4})(MEEA)]_{0.9}$	10	90	0.254
$[Li(MEEA)]_{0.2}[(P_{4,4,4,4})(MEEA)]_{0.8}$	20	80	0.572
$[Li(MEEA)]_{0.3}[(P_{4,4,4,4})(MEEA)]_{0.7}$	30	70	0.981
$[Li(MEEA)]_{0.4}[(P_{4,4,4,4})(MEEA)]_{0.6}$	40	60	1.526

Nuclear Magnetic Resonance Spectroscopy. The structure and purity of the synthesized Li-salt and ILs were characterized using a Bruker Ascend Aeon WB 400 (Bruker BioSpin AG, Fällanden, Switzerland) NMR spectrometer. $CDCl_3$ was used as a solvent. The working frequencies were 400.21 MHz for ^{1}H, 100.64 MHz for ^{13}C, 162.01 MHz for ^{31}P, and 155.53 MHz for ^{7}Li. The ^{7}Li spectra of the neat electrolytes were recorded by placing the samples in a 5 mm standard NMR tube, which was further placed inside a 10 mm standard NMR tube containing $CDCl_3$. The ^{7}Li NMR spectra were indirectly referenced to 1.0 M $LiCl_{(aq)}$. Data were processed using Bruker Topspin 3.5 software.

Pulsed Field Gradient Diffusometry. Pulsed field gradient (PFG) NMR measurements were performed on a Bruker Avance III (Bruker BioSpin AG, Fällanden, Switzerland) NMR spectrometer. The working frequencies for ^{1}H and ^{7}Li were 400.27 and 155.56 MHz, respectively. Data were processed using Bruker Topspin 3.1 software. NMR self-diffusion measurements were performed on ^{1}H and ^{7}Li with a PFG NMR probe Diff50 (Bruker) with a maximum amplitude of the magnetic field gradient pulse of 29.73 T m^{-1}. The sample was placed in a standard 5 mm glass sample tube and closed with a plastic stopper to avoid contact with air. Prior to measurements, each sample was equilibrated at a specific temperature for 30 min.

https://dx.doi.org/10.1021/acs.jpcb.0c04749
J. Phys. Chem. B 2020, 124, 9690−9700

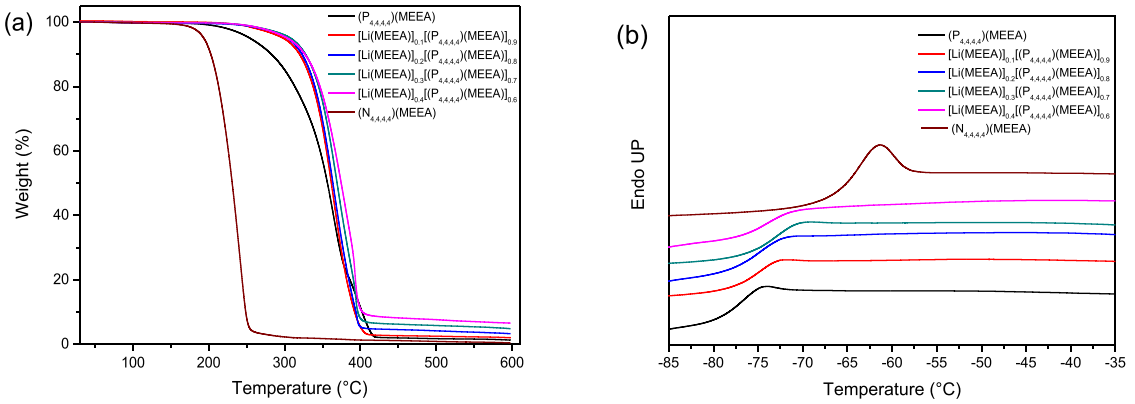

Figure 2. (a) TGA thermograms and (b) DSC traces for the neat $(N_{4,4,4,4})$(MEEA) and $(P_{4,4,4,4})$(MEEA) ILs and the $[Li(MEEA)]_x[(P_{4,4,4,4})(MEEA)]_{(1-x)}$ electrolytes. DSC traces are shifted along the y axis for clarity.

The details of the PFG NMR technique for measuring molecular diffusion coefficients can be found elsewhere.[33] A primary source of information about the diffusivity of a molecule is the diffusion decay (DD) of amplitude A of the NMR spectral line, obtained by Fourier transformation of the descending half of stimulated echo (STE), as a function of the amplitude of the applied pulsed field gradient. For a stimulated echo pulse sequence used, the diffusion decay of A in the case of a simple nonassociating molecular liquid can be described by eq 1[34]

$$A(g, \delta, t_d) = A(0)\exp(-\gamma^2 g^2 \delta^2 D t_d) \quad (1)$$

where $A(0)$ is the factor proportional to the proton content in the system and to spin−lattice and spin−spin relaxation times; γ is the gyromagnetic ratio for a used nucleus; g and δ are the amplitude and duration of the gradient pulse; t_d is the diffusion time; and D is the self-diffusion coefficient. In our experiments, t_d was in the range of 4 to 100 ms for ^{1}H diffusion, while t_d was in the range of 200 to 700 ms for ^{7}Li diffusion. No diffusion time dependence was observed in these measurements.

Infrared Spectroscopy. Attenuated total reflection−Fourier transform infrared (ATR−FTIR) spectra were recorded on a Bruker IFS 80v spectrometer equipped with a deuterated triglycine sulphate (DTGS) detector and a diamond ATR accessory. All spectra were recorded at room temperature (~22 °C) using the double-side forward−backward acquisition mode. A total number of 256 scans were coadded and signal-averaged at an optical resolution of 4 cm^{-1}.

Thermal Analysis. Thermogravimetric analysis (TGA) was performed using PerkinElmer 8000 TGA apparatus. The dynamic TGA experiments used a heating rate of 10 °C min, nitrogen gas as the inert carrier gas, and 2−4 mg of the sample. The onset of decomposition temperature, T_{onset}, was calculated from the intersection of the baseline weight and the tangent of the weight versus temperature curve using Pyris software.[35,36] Differential scanning calorimetry (DSC) was performed using PerkinElmer DSC 6000 apparatus. About 2−5 mg of the sample was packed in an aluminum pan for each experiment. DSC data were recorded during both cooling and heating traces from −100 to 100 °C at a scanning rate of 5 °C min^{-1}. The glass transition temperature, T_g, was determined as the onset of the transition. An inert nitrogen gas was supplied to the instrument at a constant flow of 20 mL min^{-1} in order to preserve a dry environment inside the sample chamber.

Electrochemical Characterization. The ESWs and the ionic conductivities were measured using a Metrohm Autolab PGSTAT302N electrochemical workstation with an FRA32M module for impedance measurements, all controlled using Nova 2.02 software. About 70 μL of the sample was placed in a sealed Microcell HC from RHD instruments. Cyclic voltammetry (CV) and linear sweep voltammetry (LSV) experiments were carried out at 20 °C temperature using a three electrode setup: 2 mm diameter glassy carbon (GC) and a platinum wire with a diameter of 0.25 mm as working electrodes (WEs), Pt crucible as a sample container as well as a counter electrode (CE), and an Ag wire coated with AgCl was used as a pseudoreference electrode (RE). The cyclic voltammograms were recorded at 100 mV s^{-1}, while the linear sweeps used were 1 mV s^{-1}. The electrochemical potentials were recorded with ferrocene as an internal reference and shifted using $E_{Li/Li^+} \approx E_{Fc/Fc^+} + 3.2$ V.[37] The ESW limits were determined using 0.1 and 0.2 mA cm^{-2} cutoff current densities.[38]

The ionic conductivities were determined from impedance measurements performed in a frequency range of 1 Hz to 1 MHz with an AC voltage amplitude of 10 mV_{rms} and from −20 to 100 ± 0.1 °C; while the heating and cooling cycles match very well (Figure S17), the data presented are taken from the heating cycles. A two-electrode setup was used with a 2 mm diameter GC WE and a 70 μL Pt crucible as a sample container as well as a CE. Both the electrodes were polished with a Kemet diamond paste 0.25 μm prior to each measurement. The cell constant was determined using a 100 μS cm^{-1} KCl standard solution from Metrohm (K_{cell} = 1.486 cm^{-1}). The cell was thermally equilibrated for at least 10 min before each measurement.

RESULTS AND DISCUSSION

For both ILs and electrolytes, we start by first assessing the phase, thermal, and electrochemical stabilities before addressing more direct LIB relevant performance parameters such as ionic conductivity and diffusion together with ion−ion interactions. A more or less complete picture of these electrolytes as promising LIB electrolytes is hereby created.

Thermal Properties. As thermal stability is one of the key properties where IL-based electrolytes are superior to conventional organic solvent-based electrolytes, all systems, $(N_{4,4,4,4})$(MEEA), $(P_{4,4,4,4})$(MEEA), and $[Li(MEEA)]_x[(P_{4,4,4,4})(MEEA)]_{(1-x)}$, were assessed by TGA and all remain stable at >200 °C and most are stable at >300 °C (Figure 2a and

https://dx.doi.org/10.1021/acs.jpcb.0c04749
J. Phys. Chem. B 2020, 124, 9690−9700

Table 2. Cathodic Limiting Potentials, Anodic Limiting Potentials, ESWs, Glass Transition Temperatures, and Thermal Decomposition Temperatures of the Neat ILs and the IL-Based Electrolytes

	0.1 mA cm^{-2}			0.2 mA cm^{-2}				
IL/electrolyte	E_C (V vs Li/Li$^+$)	E_A (V vs Li/Li$^+$)	ESW (V)	E_C (V vs Li/Li$^+$)	E_A (V vs Li/Li$^+$)	ESW (V)	T_g (°C)	T_{onset} (°C)
$(N_{4,4,4,4})$(MEEA)	2.20	5.07	2.87	1.74	5.38	3.64	−67	204
$(P_{4,4,4,4})$(MEEA)	1.11	4.75	3.64	0.88	5.0	4.12	−80	317
$[Li(MEEA)]_{0.1}[(P_{4,4,4,4})(MEEA)]_{0.9}$	1.08	4.73	3.65	0.84	4.99	4.15	−78	330
$[Li(MEEA)]_{0.2}[(P_{4,4,4,4})(MEEA)]_{0.8}$	1.07	4.87	3.80	0.82	5.08	4.26	−77	334
$[Li(MEEA)]_{0.3}[(P_{4,4,4,4})(MEEA)]_{0.7}$	0.98	4.74	3.76	0.70	5.0	4.30	−77	337
$[Li(MEEA)]_{0.4}[(P_{4,4,4,4})(MEEA)]_{0.6}$	1.06	4.81	3.75	0.69	5.20	4.51	−76	340

Table 2). While these stabilities probably are somewhat overestimated, as for more exact thermal stability determination of IL-based electrolytes, isothermal TGA must be applied,[39,40] they are anyhow highly encouraging in comparison with the standard LIB electrolyte "LP30", that is, 1 M $LiPF_6$ in EC:DMC that starts to decompose already at temperatures <100 °C with the formation of LiF and PF_5.[41] As all systems have the $(MEEA)^-$ anion in common, it is clear that the phosphonium cation is thermally more stable than the ammonium cation, which is consistent with the literature.[42,43] The addition of Li(MEEA) increases the thermal stability, more or less linearly as a function of composition and by a maximum of +23 °C for 40 mol % added.

The corresponding DSC traces reveal all systems to be glass-forming liquids, that is, they all have glass transitions (Figure 2b and Table 2). It is also clear that $(N_{4,4,4,4})$(MEEA) has a higher ionic strength and/or stronger ion−ion interactions, and thus, a higher thermal energy would be required to reach the same ionic mobility as for $(P_{4,4,4,4})$(MEEA). As expected,[44] increasing T_g values are observed as a function of Li(MEEA) addition, but they show very small increases—maximum of +3 °C for 40 mol % of Li(MEEA) (Table 2). The overall low T_g values can be attributed to the ethylene oxide units present in the $(MEEA)^-$ anion, allowing low energy rotations,[45] and for all the electrolytes, this seems to dominate over the increasing content of "hard", dynamically cross-linking Li^+ ions, which most often would cause much larger increases in T_g.[46,47]

Electrochemical Stability. The ESW of each sample is obtained from cathodic and anodic LSV experiments. The ESWs are revealed to be wider for $(P_{4,4,4,4})$(MEEA) than for $(N_{4,4,4,4})$(MEEA) (Figure 3 and Table 2). This also affects the ESWs of the electrolytes as the difference can arise only due to the IL cation. However, the widths of the ESWs (ca. 4.1−4.5 V) are anyhow quite remarkable, especially when compared to the standard LIB electrolyte, 1 M $LiPF_6$ in EC:DMC (E_C 1.3 V vs Li/Li$^+$, E_A 5.0 V vs Li/Li$^+$, and ESW 3.7 V).[48] These ESWs are comparable with the commonly studied imidazolium- and phosphonium-based ILs containing TFSI and other fluorinated anions.[49] The ESWs of all these electrolytes are narrower on the surface of the platinum electrode as compared with the GC electrode (Figure S14 and Table S1). Yet, all these ESWs should be seen as upper limits as we are using a sweep technique and the ILs are viscous; and furthermore, in a real LIB system, the electrodes might catalyze reactions earlier and hence the ESWs become narrower. By using CV, the long-term electrochemical stability and reversibility were confirmed for any electrochemical events in the neat $(P_{4,4,4,4})$(MEEA) IL and the electrolytes (Figures S11−S13). No significant changes are observed in the CV curves of $(P_{4,4,4,4})$(MEEA) IL even after 100 cycles on both GC and platinum electrode surfaces. The shoulder observed at ca. 4.8 V versus Li/Li$^+$ in the CVs is due to oxidation of a previous oxidation or reduction product of the IL.[50]

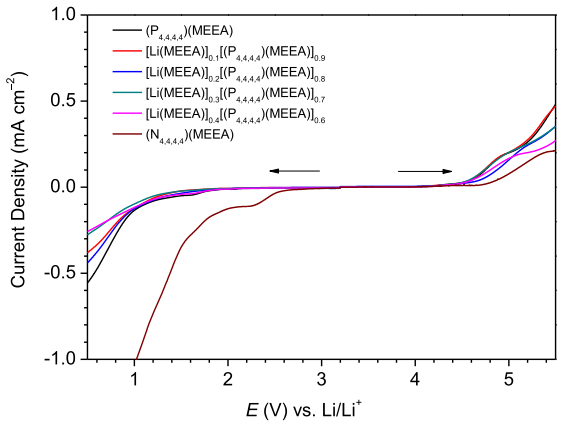

Figure 3. Linear sweep voltammetry of the neat ILs and the $[Li(MEEA)]_x[(P_{4,4,4,4})(MEEA)]_{(1-x)}$ electrolytes using GC as the WE.

Ionic Conductivity. While the ionic conductivities are always high for both neat ILs and IL-based electrolytes, it is significantly higher for $(P_{4,4,4,4})$(MEEA) than for $(N_{4,4,4,4})$-(MEEA) throughout all temperatures (Figure 4a, Table S2). It is expected because $(P_{4,4,4,4})$(MEEA) has lower viscosity and density as compared with $(N_{4,4,4,4})$(MEEA) (Figures S15 and S16). The impedance spectra of some representative samples are shown in Figures S18 and S19. For the electrolytes, the ionic conductivity, as expected, decreases as a function of the salt concentration as increasing the Li^+ concentration reduces the free volume and increases the ion−ion Coulombic interactions, primarily between the lithium ion and the $(MEEA)^-$ anion (Figure 4b, Table S2).[51,52] In addition, the Li^+ ion will most likely be coordinated with multiple $(MEEA)^-$ anions, carboxylate, and/or ether groups, leading to dynamic cross-linking and thus enhanced ion association. A similar cross-linking effect was observed when Na-salt was added to an alkoxy-ammonium-based IL.[53]

The ionic conductivities can be further analyzed by fitting the data to the Vogel−Fulcher−Tammann (VFT) equation

$$\sigma = \sigma_0 \exp\left(\frac{-B}{(T - T_0)}\right) \quad (2)$$

where σ_0, B, and T_0 are the fitting parameters, a pre-exponential factor, a factor related to the activation/pseudoactivation energy, and the dynamic glass transition temperature, respectively. The latter indicates the temperature at which the free volume is reduced so that molecular mobility

https://dx.doi.org/10.1021/acs.jpcb.0c04749
J. Phys. Chem. B 2020, 124, 9690−9700

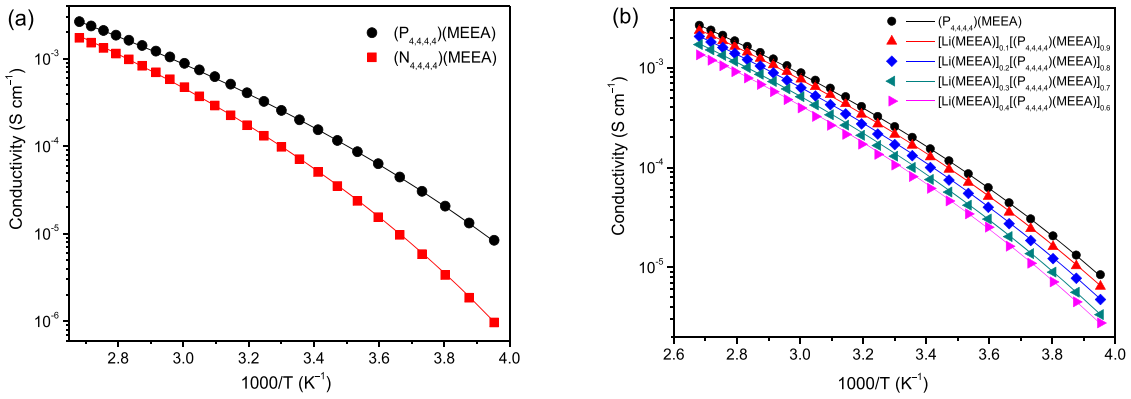

Figure 4. Ionic conductivity as a function of temperature for (a) neat ILs and (b) $[Li(MEEA)]_x[(P_{4,4,4,4})(MEEA)]_{(1-x)}$ electrolytes. The solid lines indicate the best fit of data using the Vogel−Fulcher−Tammann (VFT) equation.

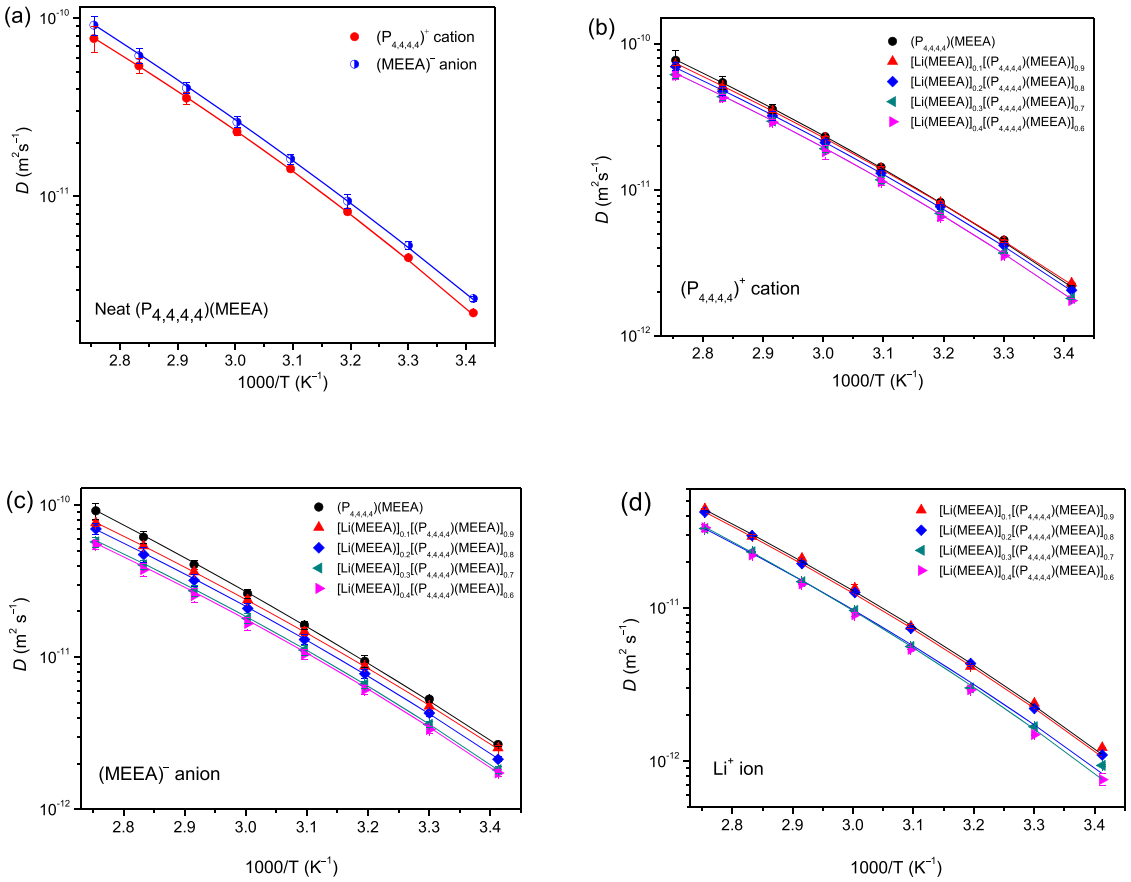

Figure 5. Diffusion coefficients of ions in (a) neat $(P_{4,4,4,4})(MEEA)$ IL and $[Li(MEEA)]_x[(P_{4,4,4,4})(MEEA)]_{(1-x)}$ electrolytes: (b) the $(P_{4,4,4,4})^+$ cation, (c) the $(MEEA)^-$ anion, and (d) Li^+ ion. The solid lines indicate the best fits of diffusion data using the VFT equation.

is arrested.[54] The activation energy for ionic conductivity (E_σ) is related to B as $E_\sigma = B{\cdot}R$. The fitting procedure was carried out over the full temperature range in two steps. In the first step, we plot $\ln(\sigma)$ versus $1/(T-T_0)$ and selected T_0 to have a linear dependence. In the second step, we fit the dependence by a linear regression to obtain the fitting parameters (σ_0, B).

The resulting VFT parameters (Table S3) show that the E_σ for $(N_{4,4,4,4})(MEEA)$ is slightly higher compared to that of $(P_{4,4,4,4})(MEEA)$, which agrees with the DSC data and again indicates that a higher thermal energy is required to reach the same ion mobility. Similarly, as expected, the E_σ increases as a function of the salt concentration for the $[Li(MEEA)]_x[(P_{4,4,4,4})(MEEA)]_{(1-x)}$ electrolytes. Building further on the comparison with the DSC data, the experimental T_g values are higher than T_0, but $T_g - T_0$ is in the range of 51−57 K and T_0/T_g is in the range of 0.71−0.75, which agree well with the empirical approximation for ILs being $T_g - T_0 \approx 50$ K and $T_0/T_g \approx 0.75$[55] and also for previously observed IL-based electrolytes.[53]

NMR Diffusometry. Having established the overall mobilities by DSC and impedance spectroscopy at a more macroscopic level, PFG NMR diffusometry was employed to better understand the mobility at the molecular level, and especially, the influence of Li^+ addition in the IL-based

https://dx.doi.org/10.1021/acs.jpcb.0c04749
J. Phys. Chem. B 2020, 124, 9690−9700

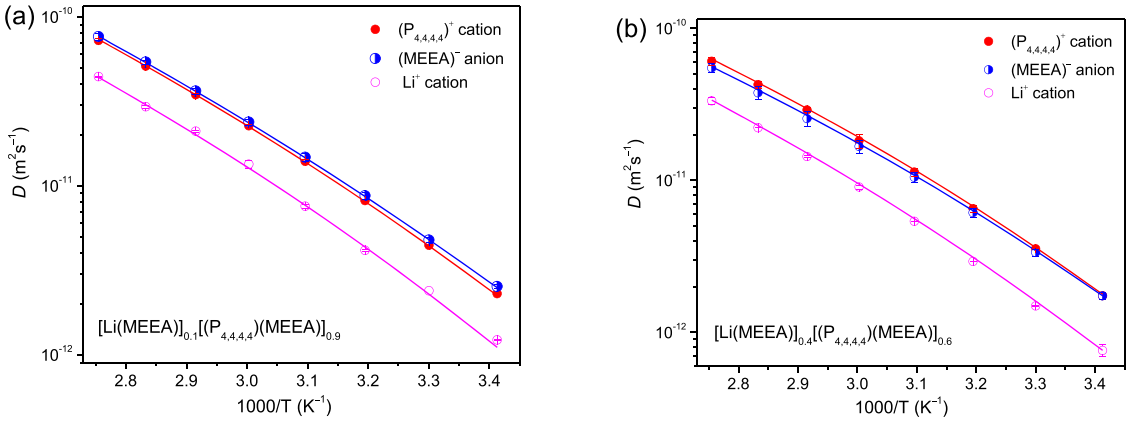

Figure 6. Diffusion coefficients of the $(P_{4,4,4,4})^+$ cation, the $(MEEA)^-$ anion, and the Li^+ ion in the (a) $[Li(MEEA)]_{0.1}[(P_{4,4,4,4})(MEEA)]_{0.9}$ and (b) $[Li(MEEA)]_{0.4}[(P_{4,4,4,4})(MEEA)]_{0.6}$ electrolytes. The solid lines indicate the best fits of diffusion data using the VFT equation.

electrolytes. The PFG NMR diffusion coefficients of all species, $(P_{4,4,4,4})^+$, $(MEEA)^-$, and Li^+ show monotonous increases as a function of temperature (Figures 5 and 6, and Table S4) and show the VFT behavior. In the case of neat $(P_{4,4,4,4})(MEEA)$, the anion diffusivity is faster than the cation diffusivity in the whole temperature range (Figure 5a), following the relative ion sizes. Upon Li-salt doping, however, while both the IL cation and anion diffusivities decrease linearly as a function of the salt concentration (Figure 5b,c), the diffusivity of the $(MEEA)^-$ anion is affected to a much greater extent, suggesting Li^+–$(MEEA)^-$ interactions. This is corroborated by the decreased diffusivity of the Li^+ ion with the increasing salt concentration (Figure 5d).

Comparing the $[Li(MEEA)]_x[(P_{4,4,4,4})(MEEA)]_{(1-x)}$ $x = 0.1$ and $x = 0.4$ electrolytes directly (Figure 6, and Figures S20 and S21) show that the diffusivities of all ions decrease with the salt concentration. For the less concentrated electrolyte, the diffusivity of $(MEEA)^-$ is still slightly higher than for $[P_{4,4,4,4}]^+$ (Figure 6a), but for the most concentrated electrolyte, it is vice versa (Figure 6b). Clearly, the Li^+ ions and the $(MEEA)^-$ anions move in a correlated fashion.

The temperature dependence of the diffusivity of ILs can be described by another VFT equation

$$D = D_0 \exp\left(\frac{-B}{(T - T_0)}\right) \tag{3}$$

where D_0, T_0, and B are adjustable parameters. The energy of activation for the diffusion of ions is associated with B as $E_D = B{\cdot}R$ and as for the ionic conductivity, the fitting procedure was carried out in two steps—with the same layout. The VFT parameters (Table S5) show that the pre-exponential factor, D_0, for the $(MEEA)^-$ anion is five times larger than for the $(P_{4,4,4,4})^+$ cation, indicating it to be the main contributor for ionic diffusivity. Although D_0 monotonically decreases for all ions with the addition of Li-salt, the effect is more prominent for the $(MEEA)^-$ anion, confirming increasing interactions between these ions. The values of T_0 estimated from the diffusion data are comparable to those calculated from the ionic conductivity data and do not change significantly with the addition of Li-salt. Similarly, the apparent activation energy for diffusion, E_D, changes slightly with the addition of Li-salt, which reveals a minor contribution in the change of ionic diffusion as compared with D_0.

The apparent transference numbers of the individual ions are determined from their diffusion coefficients in neat $(P_{4,4,4,4})(MEEA)$ and the electrolytes using the following equation[56,57]

$$t_i = \frac{x_i D_i}{\Sigma_i x_i D_i} \tag{4}$$

where t_i is the apparent transference number, x_i is the molar fraction of each individual ion, and D is the self-diffusion coefficient of an ion in $m^2\ s^{-1}$. The transference number as measured by PFG NMR is usually referred to as a transport number as the diffusion coefficients measured are averages of individual charged species, neutral species (ion pairs), and aggregates. The latter diffuse slower due to their larger radii, and this leads to lower diffusion coefficients and transference numbers—one of the reasons that transference numbers measured by electrochemical techniques are usually twice as large.[58]

The apparent transference numbers (t_i) of Li^+, $(P_{4,4,4,4})^+$, and $(MEEA)^-$ ions as a function of the Li-salt concentration and temperature show that the $(MEEA)^-$ anion moves faster than the $(P_{4,4,4,4})^+$ cation (Figure 7, Table S6). The transference number of Li^+ increases linearly with the increasing Li-salt concentration, while it decreases for the $(P_{4,4,4,4})^+$ cation, which is attributed to the increasing/decreasing number densities.[59] However, no significant changes are seen for the $(MEEA)^-$ anion.

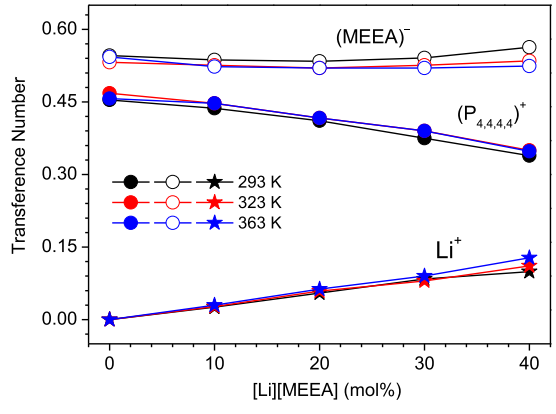

Figure 7. Apparent transfer numbers of ions in neat $(P_{4,4,4,4})(MEEA)$ and $[Li(MEEA)]_x[(P_{4,4,4,4})(MEEA)]_{(1-x)}$ electrolytes.

https://dx.doi.org/10.1021/acs.jpcb.0c04749
J. Phys. Chem. B 2020, 124, 9690–9700

The ratio of the molar conductivity obtained from the impedance measurements (Λ_{imp}) and the molar conductivity calculated from the diffusion coefficients of ions (Λ_{NMR}) is commonly used to investigate the ionic association and dissociation under equilibrium in RTILs. The $\Lambda_{imp}/\Lambda_{NMR}$ ratio indicates the percentages of ions responsible for the ion conduction within the diffusing unit, that is, the ionicity.[60] Here, the $\Lambda_{imp}/\Lambda_{NMR}$ ratio for neat $(P_{4,4,4,4})$(MEEA) is investigated as a function of temperature (Figure S26). The molar conductivity is calculated from the self-diffusion coefficients using the Nernst−Einstein equation:[61]

$$\Lambda_{NMR} = F^2(D_{cation} + D_{anion})/RT \quad (5)$$

where F is the Faraday constant and R is the universal gas constant.

The $\Lambda_{imp}/\Lambda_{NMR}$ ratio being lower than unity indicates the presence of ionic association and that only a fraction of the diffusing species contributes to the ionic conduction.[62] The ratio decreases as a function of temperature showing more ionic association, which is sensitive to temperature, as expected.[63]

^{7}Li NMR Spectroscopy. ^{7}Li NMR spectroscopy was employed to get further insights into the local environment of the Li^+ ions and the interactions with the $(MEEA)^-$ anions. Both the chemical shift and the line width change upon the addition of Li-salt, suggesting that the local environment changes as well (Figure 8). The downshifts in the ^{7}Li NMR

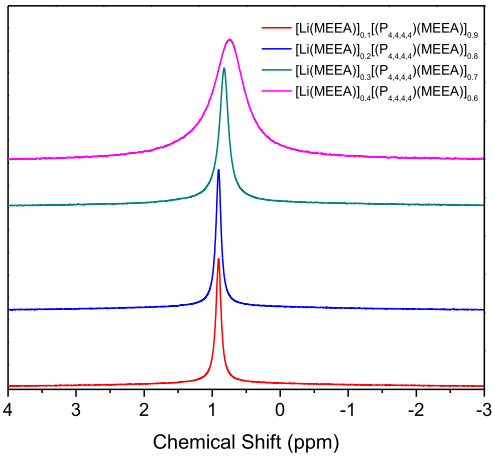

Figure 8. ^{7}Li NMR spectra of the $[Li(MEEA)]_x[(P_{4,4,4,4})(MEEA)]_{(1-x)}$ electrolytes.

spectra agree with previous observations for LiFSI-doped $(C_3mpyr)(FSI)$.[64] In contrast, the ^{31}P NMR spectra show only a single resonance line for the $(P_{4,4,4,4})^+$ cation, suggesting no significant changes (Figures S22−S25), most likely due to the fact that the alkyl chains wrap around and shield the cation positive center from the anion. The line widths of the ^{7}Li NMR spectra increase with the salt concentration and as the homogeneous NMR line broadening is determined by the molecular motions,[65] it reveals that the lithium ions become less mobile in the electrolytes with higher salt concentrations, which is in accordance with both the ionic conductivity and the ion diffusivity data.

Infrared Spectroscopy. To get an additional and deeper insight into the ion−ion interactions, FTIR spectroscopy was applied, and especially in the regions of the asymmetric and the symmetric stretching bands of the carboxylate group of $(MEEA)^-$, we expect relevant features. In the former region, there is, for $(P_{4,4,4,4})$(MEEA), a main band at 1673 cm^{-1} with distinct satellite bands on both sides at 1713 and 1609 cm^{-1}, indicating several different types of coordination/interaction active sites, while for $(N_{4,4,4,4})$(MEEA), there is a single, albeit broad, feature at 1725 cm^{-1}, which is more similar to a clear carbonyl group interaction (Figure 9a).[66] The symmetric stretching band of the carboxylate group appears as a single and symmetrical peak at 1463 cm^{-1} for $(P_{4,4,4,4})$(MEEA) and for $(N_{4,4,4,4})$(MEEA) also with a shoulder at 1489 cm^{-1}, again suggesting stronger interactions with the carboxylate group. The stronger and single mode of interaction also agrees well with the lower ionic conductivity of $(N_{4,4,4,4})$(MEEA).

Looking further at the spectral regions sensitive to the oligoether functional groups of the $(MEEA)^-$ anion, a C−O stretching band appears at 1099 cm^{-1} for $(P_{4,4,4,4})$(MEEA) and it is slightly upshifted for $(N_{4,4,4,4})$(MEEA) (Figure 9b). At the lower wavenumbers in the range of 900 to 800 cm^{-1}, the infrared absorptions represent a mixture of CH_2 rocking and CO stretching motions.[67] These vibrations are rather sensitive to any structural changes and shift upon interactions with a counter cation.[68] The absorption bands at 850 and 817 cm^{-1} for $(P_{4,4,4,4})$(MEEA) IL are shifted toward higher wavenumbers at 879 and 853 cm^{-1} for $(N_{4,4,4,4})$(MEEA) IL, suggesting much stronger interactions of the $(MEEA)^-$ anion with the $(N_{4,4,4,4})^+$ cation than the $(P_{4,4,4,4})^+$ cation. A comparison of the full range FTIR spectra of neat $(P_{4,4,4,4})$(MEEA) and $(N_{4,4,4,4})$(MEEA) ILs is shown in Figure S27.

The addition of Li(MEEA) to $(P_{4,4,4,4})$(MEEA) changes the interactions; the bands at 1713 and 1673 cm^{-1} both disappear and the peak at 1609 cm^{-1} increases, which also is approximately the region of the pure Li(MEEA) salt feature (Figure 9c). This change clearly shows that the Li^+ ion interacts strongly with the carboxylate group of the $(MEEA)^-$ anion, but the symmetric stretching band region is much difficult to analyze. In contrast, neither the C−O bond stretching region nor the 800−1000 cm^{-1} region changes to any large extent (Figure 9d) although significant changes have previously been observed in this region for mixtures of various oligoethers and alkali metal salts.[69−71] Here the Li^+ ions seem to be only weakly interacting with the oxygen atoms of the ethylene oxide units of the $(MEEA)^-$ anion. The only major differences are increases in the intensity of the C−O stretching band at around 1100 cm^{-1} as a function of the Li(MEEA) concentration, quite naturally as it induces relatively higher $(MEEA)^-$ concentrations. This picture of the cation coordination is in support of the DSC analysis, suggesting that the addition of Li(MEEA) has a negligible effect on the flexibility of the oligoether backbone within the $(MEEA)^-$ anion, which is also in great accordance with the findings for the alkali metal salts of the 2,5,8,11-tetraoxatridecan-13-oate anion, $(TOTO)^-$, which is a rather similar anion, showing strong coordination with the carboxylate group and moderate interactions with the oligoether groups.[72]

CONCLUSIONS

Among the neat ILs, $(P_{4,4,4,4})$(MEEA) has more beneficial properties than $(N_{4,4,4,4})$(MEEA) such as much better thermal and electrochemical stabilities, a lower glass transition temperature, and higher ionic conductivity. As is not uncommon to IL-based electrolytes, both the total ionic conductivity and the diffusivity of the Li^+ ions decrease as a function of the salt concentration. The local coordination

https://dx.doi.org/10.1021/acs.jpcb.0c04749
J. Phys. Chem. B 2020, 124, 9690−9700

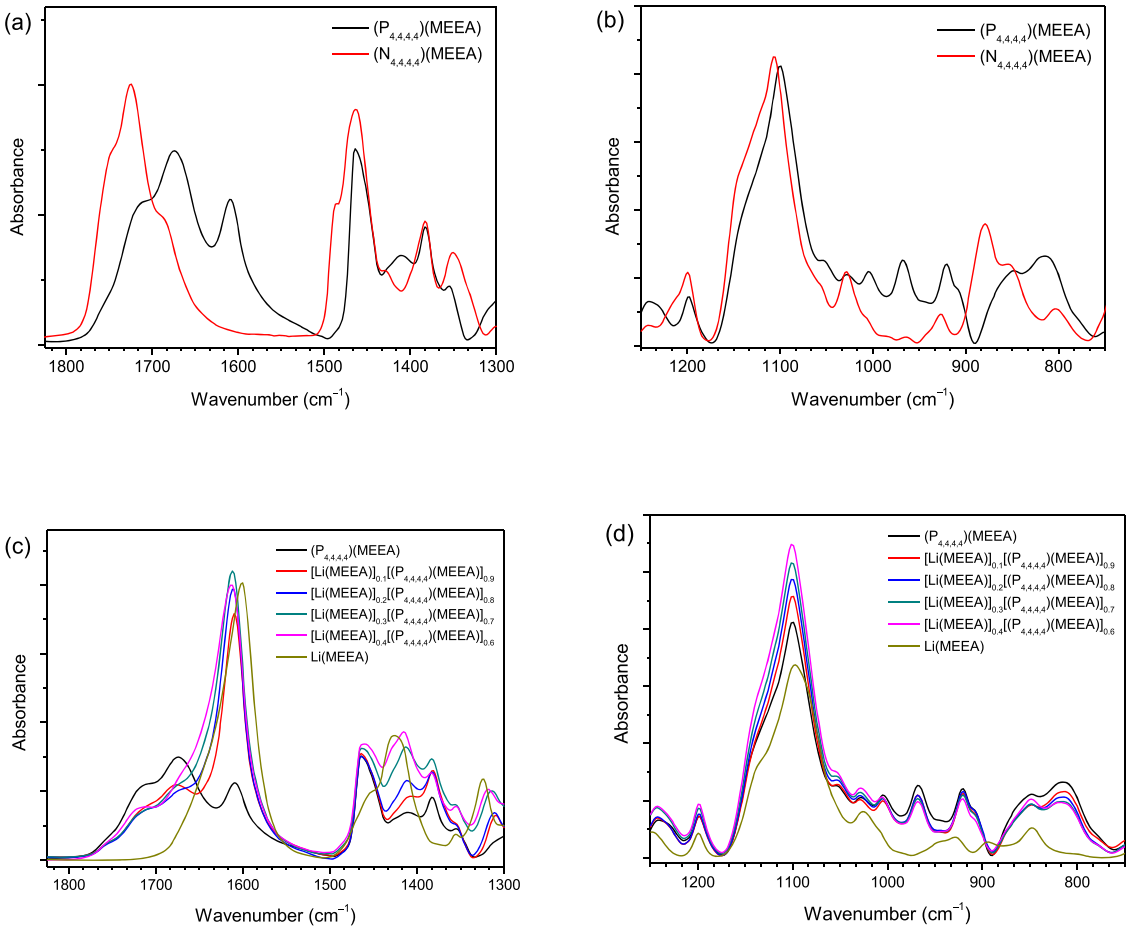

Figure 9. FTIR spectra of the (a and b) neat $(N_{4,4,4,4})$(MEEA) and $(P_{4,4,4,4})$(MEEA) ILs and (c and d) $(P_{4,4,4,4})$(MEEA), Li(MEEA), and the $[Li(MEEA)]_x[(P_{4,4,4,4})(MEEA)]_{(1-x)}$ electrolytes.

points to strong ion−ion interactions, albeit to a very varying degree for the three different cations, with the $(MEEA)^-$ anion—but all primarily with the carboxylate group. Altogether, while the strong cation−anion interactions might be less beneficial in terms of charge carrier concentration and in terms of creating a dynamically cross-linked structure, they render the high flexibility of the oligoethylene glycol moiety of the $(MEEA)^-$ anion intact—and hence more globally dynamic electrolytes, as seen by the small changes induced in the glass transition temperatures. The combination of the latter and FTIR data revealed that ion−ion interactions can even be used to look at how the different IL cations interact with the $(MEEA)^-$ anion. Overall, the here created IL-based electrolytes have promising potential to be used in batteries operating over a wide range of temperature and electrochemical potential.

■ ASSOCIATED CONTENT

Supporting Information

The Supporting Information is available free of charge at https://pubs.acs.org/doi/10.1021/acs.jpcb.0c04749.

Synthesis of the lithium salt and the ionic liquids; ^1H, ^{13}C, ^{31}P, and ^7L NMR spectra; CV and LSV curves; dynamic viscosity and density of neat $(P_{4,4,4,4})$(MEEA)- and $(P_{4,4,4,4})$(MEEA) ILs; heating and cooling cycles of the ionic conductivity of $(P_{4,4,4,4})$(MEEA); Nyquist plots; comparison of the diffusivity of ions; ^{31}P NMR spectra of the neat electrolytes; ratio of molar conductivities measured by impedance and NMR spectroscopies, FTIR spectra of neat $(P_{4,4,4,4})$(MEEA) and $(N_{4,4,4,4})$(MEEA) ILs; Tables of cathodic limiting potentials, anodic limiting potentials, and ESWs; ionic conductivity; VFT equation parameters; diffusivity data; and transference numbers of the ionic liquids and the electrolytes (PDF)

■ AUTHOR INFORMATION

Corresponding Authors

Faiz Ullah Shah − *Chemistry of Interfaces, Luleå University of Technology, SE-971 87 Luleå, Sweden;* orcid.org/0000-0003-3652-7798; Email: faiz.ullah@ltu.se

Patrik Johansson − *Department of Physics, Chalmers University of Technology, SE-412 96 Gothenburg, Sweden; ALISTORE-European Research Institute, 80039 Amiens, France;* orcid.org/0000-0002-9907-117X; Email: patrik.johansson@chalmers.se

Authors

Oleg I. Gnezdilov − *Institute of Physics, Kazan Federal University, 420008 Kazan, Russia*

Inayat Ali Khan − *Chemistry of Interfaces, Luleå University of Technology, SE-971 87 Luleå, Sweden;* orcid.org/0000-0002-7940-7297

Andrei Filippov − *Chemistry of Interfaces, Luleå University of Technology, SE-971 87 Luleå, Sweden; Medical and Biological*

Physics, Kazan Medical University, 420012 Kazan, Russia; orcid.org/0000-0002-6810-1882

Natalia A. Slad − *Institute of Polymers, Kazan National Research Technological University, 420015 Kazan, Russia*

Complete contact information is available at: https://pubs.acs.org/10.1021/acs.jpcb.0c04749

Notes

The authors declare no competing financial interest.

■ ACKNOWLEDGMENTS

The financial support from the Swedish Research Council (project number: 2018-04133) is gratefully acknowledged. P.J. is grateful for the continuous support from the Chalmers Areas of Advance Materials Science, Energy, and Transport. O.I.G. acknowledges the subsidy allocated to the Kazan Federal University for the state assignment in the sphere of scientific activities (project number: 0671-2020-0051).

■ REFERENCES

(1) Xu, K. Electrolytes and interphases in Li-ion batteries and beyond. *Chem. Rev.* **2014**, *114*, 11503−11618.
(2) Matsuda, Y.; Morita, M.; Yamashita, T. Conductivity of the $LiBF_4$/mixed ether electrolytes for secondary lithium cells. *J. Electrochem. Soc.* **1984**, *131*, 2821−2827.
(3) Hammami, A.; Raymond, N.; Armand, M. Runaway risk of forming toxic compounds. *Nature* **2003**, *424*, 635−636.
(4) Tsuzuki, S.; Shinoda, W.; Seki, S.; Umebayashi, Y.; Yoshida, K.; Dokko, K.; Watanabe, M. Intermolecular interactions in Li^+-glyme and Li^+-glyme−$TFSA^-$ complexes: relationship with physicochemical properties of [Li(glyme)][TFSA] ionic liquids. *ChemPhysChem* **2013**, *14*, 1993−2001.
(5) Westman, K.; Dugas, R.; Jankowski, P.; Wieczorek, W.; Gachot, G.; Morcrette, M.; Irisarri, E.; Ponrouch, A.; Palacín, M. R.; Tarascon, J.-M.; Johansson, P. Diglyme based electrolytes for sodium-ion batteries. *ACS Appl. Energy Mater.* **2018**, *1*, 2671−2680.
(6) Fang, S.; Wang, G.; Qu, L.; Luo, D.; Yang, L.; Hirano, S. A novel mixture of diethylene glycol diethylether and non-flammable methyl-nonafluorobutyl ether as a safe electrolyte for lithium ion batteries. *J. Mater. Chem. A* **2015**, *3*, 21159−21166.
(7) Ueno, K.; Yoshida, K.; Tsuchiya, M.; Tachikawa, N.; Dokko, K.; Watanabe, M. Glyme−lithium salt equimolar molten mixtures: concentrated solutions or solvate ionic liquids? *J. Phys. Chem. B* **2012**, *116*, 11323−11331.
(8) Ueno, K.; Murai, J.; Ikeda, K.; Tsuzuki, S.; Tsuchiya, M.; Tatara, R.; Mandai, T.; Umebayashi, Y.; Dokko, K.; Watanabe, M. Li^+ solvation and ionic transport in lithium solvate ionic liquids diluted by molecular solvents. *J. Phys. Chem. C* **2016**, *120*, 15792−15802.
(9) Kim, H.; Hong, J.; Park, Y.-U.; Kim, J.; Hwang, I.; Kang, K. Sodium storage behavior in natural graphite using ether based electrolyte systems. *Adv. Funct. Mater.* **2015**, *25*, 534−541.
(10) Zhu, Z.; Cheng, F.; Hu, Z.; Niu, Z.; Chen, J. Highly stable and ultrafast electrode reaction of graphite for sodium ion batteries. *J. Power Sources* **2015**, *293*, 626−634.
(11) Black, R.; Oh, S. H.; Lee, J.-H.; Yim, T.; Adams, B.; Nazar, L. F. Screening for superoxide reactivity in Li-O_2 batteries: effect on Li_2O_2/LiOH crystallization. *J. Am. Chem. Soc.* **2012**, *134*, 2902−2905.
(12) Seh, Z. W.; Sun, J.; Sun, Y.; Cui, Y. A Highly reversible room-temperature sodium metal anode. *ACS Cent. Sci.* **2015**, *1*, 449−455.
(13) Jache, B.; Binder, J. O.; Abe, T.; Adelhelm, P. A comparative study on the impact of different glymes and their derivatives as electrolyte solvents for graphite co-intercalation electrodes in lithium-ion and sodium-ion batteries. *Phys. Chem. Chem. Phys.* **2016**, *18*, 14299−14316.
(14) MacFarlane, D. R.; Tachikawa, N.; Forsyth, M.; Pringle, J. M.; Howlett, P. C.; Elliott, G. D.; Davis, J. H., Jr.; Watanabe, M.; Simon, P.; Angell, C. A. Energy applications of ionic liquids. *Energy Environ. Sci.* **2014**, *7*, 232−250.
(15) Jankowski, P.; Wieczorek, W.; Johansson, P. Functional ionic liquids: cationic SEI-formers for lithium batteries. *Energy Storage Mater.* **2019**, *20*, 108−117.
(16) Wilken, S.; Xiong, S.; Scheers, J.; Jacobsson, P.; Johansson, P. Ionic liquids in lithium battery electrolytes: composition versus safety and physical properties. *J. Power Sources* **2015**, *275*, 935−942.
(17) Forsyth, M.; Porcarelli, L.; Wang, X.; Goujon, N.; Mecerreyes, D. Innovative electrolytes based on ionic liquids and polymers for next-generation solid-state batteries. *Acc. Chem. Res.* **2019**, *52*, 686−694.
(18) Xing, H.; Liao, C.; Yang, Q.; Veith, G. M.; Guo, B.; Sun, X. G.; Ren, Q.; Hu, Y. S.; Dai, S. Ambient lithium−SO_2 batteries with ionic liquids as electrolytes. *Angew. Chem., Int. Ed.* **2014**, *53*, 2099−2103.
(19) Xia, L.; Yu, L.; Hu, D.; Chen, G. Z. Electrolytes for electrochemical energy storage. *Mater. Chem. Front.* **2017**, *1*, 584−618.
(20) Watanabe, M.; Thomas, M. L.; Zhang, S.; Ueno, K.; Yasuda, T.; Dokko, K. Application of ionic liquids to energy storage and conversion materials and devices. *Chem. Rev.* **2017**, *117*, 7190−7239.
(21) Giffin, G. A. Ionic liquid-based electrolytes for "beyond lithium" battery technologies. *J. Mater. Chem. A* **2016**, *4*, 13378−13389.
(22) Lewandowski, A.; Świderska-Mocek, A. Ionic liquids as electrolytes for Li-ion batteries-an overview of electrochemical studies. *J. Power Sources* **2009**, *194*, 601−609.
(23) Bhatt, A. I.; Best, A. S.; Huang, J.; Hollenkamp, A. F. Application of the *N*-propyl-*N*-methyl-pyrrolidinium bis(fluorosulfonyl)imide RTIL containing lithium bis(fluorosulfonyl)imide in ionic liquid based lithium batteries. *J. Electrochem. Soc.* **2010**, *157*, A66−A74.
(24) Budi, A.; Basile, A.; Opletal, G.; Hollenkamp, A. F.; Best, A. S.; Rees, R. J.; Bhatt, A. I.; O'Mullane, A. P.; Russo, S. P. Study of the initial stage of solid electrolyte interphase formation upon chemical reaction of lithium metal and *N*-methyl-*N*-propyl-pyrrolidinium-bis(fluorosulfonyl)imide. *J. Phys. Chem. C* **2012**, *116*, 19789−19797.
(25) Lane, G. H.; Bayley, P. M.; Clare, B. R.; Best, A. S.; MacFarlane, D. R.; Forsyth, M.; Hollenkamp, A. F. Ionic liquid electrolyte for lithium metal batteries: physical, electrochemical, and interfacial studies of *N*-methyl-*N*-butylmorpholinium bis(fluorosulfonyl)imide. *J. Phys. Chem. C* **2010**, *114*, 21775−21785.
(26) Sakaebe, H.; Matsumoto, H. *N*-Methyl-*N*-propylpiperidinium bis(trifluoromethanesulfonyl)imide (PP13−TFSI) − novel electrolyte base for Li battery. *Electrochem. Commun.* **2003**, *5*, 594−598.
(27) Girard, G. M. A.; Hilder, M.; Nucciarone, D.; Whitbread, K.; Zavorine, S.; Moser, M.; Forsyth, M.; MacFarlane, D. R.; Howlett, P. C. Role of Li concentration and the SEI layer in enabling high performance Li metal electrodes using a phosphonium bis(fluorosulfonyl)imide ionic liquid. *J. Phys. Chem. C* **2017**, *121*, 21087−21095.
(28) Giri, S.; Behera, S.; Jena, P. Superhalogens as building blocks of halogen-free electrolytes in lithium-ion batteries. *Angew. Chem.* **2014**, *126*, 14136−14139.
(29) Monteiro, M. J.; Camilo, F. F.; Ribeiro, M. C. C.; Torresi, R. M. Ether-bond-containing ionic liquids and the relevance of the ether bond position to transport properties. *J. Phys. Chem. B* **2010**, *114*, 12488−12494.
(30) Blundell, R. K.; Licence, P. Quaternary ammonium and phosphonium based ionic liquids: a comparison of common anions. *Phys. Chem. Chem. Phys.* **2014**, *16*, 15278−15288.
(31) Carvalho, P. J.; Ventura, S. P. M.; Batista, M. L. S.; Schröder, B.; Gonçalves, F.; Esperança, J.; Mutelet, F.; Coutinho, J. A. P. Understanding the impact of the central atom on the ionic liquid behavior: phosphonium vs ammonium cations. *J. Chem. Phys.* **2014**, *140*, No. 064505.
(32) Zech, O.; Kellermeier, M.; Thomaier, S.; Maurer, E.; Klein, R.; Schreiner, C.; Kunz, W. Alkali metal oligoether carboxylates-a new class of ionic liquids. *Chem. − Eur. J.* **2009**, *15*, 1341−1345.

(33) Callaghan, P. T. *Principles of nuclear magnetic resonance microscopy; Clarendon press*; Oxford, 1991.
(34) Tanner, J. E. Use of the stimulated echo in NMR diffusion studies. *J. Chem. Phys.* **1970**, *52*, 2523−2526.
(35) Fredlake, C. P.; Crosthwaite, J. M.; Hert, D. G.; Aki, S. N. V. K.; Brennecke, J. F. Thermophysical properties of imidazolium-based ionic liquids. *J. Chem. Eng. Data* **2004**, *49*, 954−964.
(36) Maton, C.; de Vos, N.; Stevens, C. V. Ionic liquid thermal stabilities: decomposition mechanisms and analysis tools. *Chem. Soc. Rev.* **2013**, *42*, 5963−5977.
(37) Neale, A. R.; Murphy, S.; Goodrich, P.; Hardacre, C.; Jacquemin, J. Thermophysical and electrochemical properties of ethereal functionalised cyclic alkylammonium-based ionic liquids as potential electrolytes for electrochemical applications. *ChemPhysChem* **2017**, *18*, 2040−2057.
(38) Xue, Z.; Qin, L.; Jiang, J.; Mu, T.; Gao, G. Thermal, electrochemical and radiolytic stabilities of ionic liquids. *Phys. Chem. Chem. Phys.* **2018**, *20*, 8382−8402.
(39) Kerner, M.; Johansson, P. Pyrrolidinium FSI and TFSI based polymerized ionic liquids as electrolytes for high temperature lithium-ion batteries. *Batteries* **2018**, *4*, 10.
(40) Oltean, G.; Plylahan, N.; Ihrfors, C.; Wei, W.; Xu, C.; Edström, K.; Nyholm, L.; Johansson, P.; Gustafsson, T. Towards Li-ion batteries operating at 80 °C: Ionic liquid versus conventional liquid electrolytes. *Batteries* **2018**, *4*, 2.
(41) Arbizzani, C.; Gabrielli, G.; Mastragostino, M. Thermal stability and flammability of electrolytes for lithium-ion batteries. *J. Power Sources* **2011**, *196*, 4801−4805.
(42) Tsunashima, K.; Niwa, E.; Kodama, S.; Sugiya, M.; Ono, Y. Thermal and transport properties of ionic liquids based on benzyl-substituted phosphonium cations. *J. Phys. Chem. B* **2009**, *113*, 15870−15874.
(43) Shirota, H.; Fukazawa, H.; Fujisawa, T.; Wishart, J. F. Heavy atom substitution effects in non-aromatic ionic liquids: ultrafast dynamics and physical properties. *J. Phys. Chem. B* **2010**, *114*, 9400−9412.
(44) Kerner, M.; Plylahan, N.; Scheers, J.; Johansson, P. Ionic liquid based lithium battery electrolytes: fundamental benefits of utilising both TFSI and FSI anions? *Phys. Chem. Chem. Phys.* **2015**, *17*, 19569−19581.
(45) Klein, R.; Zech, O.; Maurer, E.; Kellermeier, M.; Kunz, W. Oligoether carboxylates: task-Specific room-temperature ionic liquids. *J. Phys. Chem. B* **2011**, *115*, 8961−8969.
(46) Girard, G. M. A.; Hilder, M.; Zhu, H.; Nucciarone, D.; Whitbread, K.; Zavorine, S.; Moser, M.; Forsyth, M.; MacFarlane, D. R.; Howlett, P. C. Electrochemical and physicochemical properties of small phosphonium cation ionic liquid electrolytes with high lithium salt content. *Phys. Chem. Chem. Phys.* **2015**, *17*, 8706−8713.
(47) Gao, X.; Wu, F.; Mariani, A.; Passerini, S. Concentrated ionic-liquid-based electrolytes for high-voltage lithium batteries with improved performance at room temperature. *ChemSusChem* **2019**, *12*, 4185−4193.
(48) Goodenough, J. B.; Kim, Y. Challenges for rechargeable Li batteries. *Chem. Mater.* **2010**, *22*, 587−603.
(49) Barrosse-Antle, L. E.; Bond, A. M.; Compton, R. G.; O'Mahony, A. M.; Rogers, E. I.; Silvester, D. S. Voltammetry in room temperature ionic liquids: comparisons and contrasts with conventional electrochemical solvents. *Chem. − Asian J.* **2010**, *5*, 202−230.
(50) Tsunashima, K.; Sugiya, M. Physical and electrochemical properties of low-viscosity phosphonium ionic liquids as potential electrolytes. *Electrochem. Commun.* **2007**, *9*, 2353−2358.
(51) Shah, F. U.; Gnezdilov, O.; Filippov, A. Ion dynamics in halogen-free phosphonium bis(salicylato)borate ionic liquid electrolytes for lithium-ion batteries. *Phys. Chem. Chem. Phys.* **2017**, *19*, 16721−16730.
(52) Shah, F. U.; Gnezdilov, O. I.; Gusain, R.; Filippov, A. Transport and association of ions in lithium battery electrolytes based on glycol ether mixed with halogen-free orthoborate ionic liquid. *Sci. Rep.* **2017**, *7*, 16340.
(53) Pope, C. R.; Kar, M.; MacFarlane, D. R.; Armand, M.; Forsyth, M.; O'Dell, L. A. Ion dynamics in a mixed-cation alkoxy-ammonium ionic liquid electrolyte for sodium device applications. *ChemPhysChem* **2016**, *17*, 3187−3195.
(54) Cohen, M. H.; Turnbull, D. Molecular transport in liquids and gases. *J. Chem. Phys.* **1959**, *31*, 1164−1169.
(55) Galiński, M.; Lewandowski, A.; Stępniak, I. Ionic liquids as electrolytes. *Electrochim. Acta* **2006**, *51*, 5567−5580.
(56) Frömling, T.; Kunze, M.; Schönhoff, M.; Sundermeyer, J.; Roling, B. Enhanced lithium transference numbers in ionic liquid electrolytes. *J. Phys. Chem. B* **2008**, *112*, 12985−12990.
(57) Gélinas, B.; Natali, M.; Bibienne, T.; Li, Q. P.; Dollé, M.; Rochefort, D. Electrochemical and transport properties of ions in mixtures of electroactive ionic liquid and propylene carbonate with a lithium salt for lithium-ion batteries. *J. Phys. Chem. C* **2016**, *120*, 5315−5325.
(58) Martins, V. L.; Sanchez-Ramirez, N.; Ribeiro, M. C. C.; Torresi, R. M. Two phosphonium ionic liquids with high Li+ transport number. *Phys. Chem. Chem. Phys.* **2015**, *17*, 23041−523051.
(59) Brinkkötter, M.; Giffin, G. A.; Moretti, A.; Jeong, S.; Passerini, S.; Schönhoff, M. Relevance of ion clusters for Li transport at elevated salt concentrations in $[Pyr_{12O1}][FTFSI]$ ionic liquid-based electrolytes. *Chem. Commun.* **2018**, *54*, 4278−4281.
(60) Tokuda, H.; Hayamizu, K.; Ishii, K.; Susan, M. A. B. H.; Watanabe, M. Physicochemical properties and structures of room temperature ionic liquids. 2. Variation of alkyl chain length in imidazolium cation. *J. Phys. Chem. B* **2005**, *109*, 6103−6110.
(61) Tokuda, H.; Hayamizu, K.; Ishii, K.; Susan, M. A. B. H.; Watanabe, M. Physicochemical properties and structures of room temperature ionic liquids. 1. Variation of anionic species. *J. Phys. Chem. B* **2004**, *108*, 16593−16600.
(62) Aihara, Y.; Sugimoto, K.; Price, W. S.; Hayamizu, K. Ionic conduction and self-diffusion near infinitesimal concentration in lithium salt-organic solvent electrolytes. *J. Chem. Phys.* **2000**, *113*, 1981−1991.
(63) Seki, S.; Hayamizu, K.; Tsuzuki, S.; Fujii, K.; Umebayashi, Y.; Mitsugi, T.; Kobayashi, T.; Ohno, Y.; Kobayashi, Y.; Mita, Y.; Miyashiro, H.; Ishiguro, S. I. Relationships between center atom species (N, P) and ionic conductivity, viscosity, density, self-diffusion coefficient of quaternary cation room-temperature ionic liquids. *Phys. Chem. Chem. Phys.* **2009**, *11*, 3509−3514.
(64) Yoon, H.; Best, A. S.; Forsyth, M.; MacFarlane, D. R.; Howlett, P. C. Physical properties of high Li-ion content *N*-propyl-*N*-methylpyrrolidinium bis(fluorosulfonyl)imide based ionic liquid electrolytes. *Phys. Chem. Chem. Phys.* **2015**, *17*, 4656−4663.
(65) Levitt, M. *Spin Dynamics. Basics of nuclear magnetic resonance* (2nd Ed); Wiley & Sons: New York, 2008.
(66) Shah, F. U.; Holmgren, A.; Rutland, M. W.; Glavatskih, S.; Antzutkin, O. N. Interfacial behavior of orthoborate ionic liquids at inorganic oxide surfaces probed by NMR, IR and Raman spectroscopy. *J. Phys. Chem. C* **2018**, *122*, 19687−19698.
(67) Frech, R.; Huang, W. Conformational changes in diethylene glycol dimethyl ether and poly(ethylene oxide) induced by lithium ion complexation. *Macromolecules* **1995**, *28*, 1246−1251.
(68) Brouillette, D.; Irish, D. E.; Taylor, N. J.; Perron, G.; Odziemkowski, M.; Desnoyers, J. E. Stable solvates in solution of lithium bis(trifluoromethylsulfone)imide in glymes and other aprotic solvents: phase diagrams, crystallography and Raman spectroscopy. *Phys. Chem. Chem. Phys.* **2002**, *4*, 6063−6071.
(69) Johansson, P.; Grondin, J.; Lassègues, J. C. Structural and vibrational properties of diglyme and longer glymes. *J. Phys. Chem. A* **2010**, *114*, 10700−10705.
(70) Gejji, S. P.; Johansson, P.; Tegenfeldt, J.; Lindgren, J. Conformational changes induced by metal ion coordination: Lithium-(I) − Diglyme. *Comput. Polym. Sci.* **1995**, *5*, 99−105.
(71) Johansson, P.; Gejji, S. P.; Tegenfeldt, J.; Lindgren, J. Local coordination and conformation in polyether electrolytes: geometries

https://dx.doi.org/10.1021/acs.jpcb.0c04749
J. Phys. Chem. B 2020, 124, 9690−9700

of M-triglyme complexes (M = Li, Na, K, Mg and Ca) from ab-initio molecular orbital calculations. *Solid State Ionics* **1996**, *86-88*, 297−302.

(72) Zech, O.; Hunger, J.; Sangoro, J. R.; Iacob, C.; Kremer, F.; Kunz, W.; Buchner, R. Correlation between polarity parameters and dielectric properties of [Na][TOTO]−a sodium ionic liquid. *Phys. Chem. Chem. Phys.* **2010**, *12*, 14341−14350.

https://dx.doi.org/10.1021/acs.jpcb.0c04749
J. Phys. Chem. B 2020, 124, 9690−9700